tvst

Article

Angiopoietin-1 Knockout Mice as a Genetic Model of Open-Angle Glaucoma

Benjamin R. Thomson[1,*], Marta Grannonico[2,*], Feng Liu[2,3], Mingna Liu[2], Parrykumar Mendapara[1], Ying Xu[3], Xiaorong Liu[2,4], and Susan E. Quaggin[1]

[1] Feinberg Cardiovascular and Renal Research Institute and Division of Nephrology and Hypertension, Northwestern University Feinberg School of Medicine, Chicago, IL, USA
[2] Department of Biology, University of Virginia, Charlottesville, VA, USA
[3] Guangdong-Hong Kong-Macau Institute of CNS Regeneration, Ministry of Education CNS Regeneration Collaborative Joint Laboratory, Jinan University, Guangzhou, China
[4] Department of Psychology, University of Virginia, Charlottesville, VA, USA

Correspondence: Susan E. Quaggin, Feinberg Cardiovascular and Renal Research Institute, Northwestern University, 303 E Superior St, Suite 10-105, Chicago, IL, 60611, USA.
e-mail: quaggin@northwestern.edu

Received: July 12, 2019
Accepted: January 6, 2020
Published: March 18, 2020

Keywords: glaucoma; angiopoietin; animal model

Citation: Thomson BR, Grannonico M, Liu F, Liu M, Mendapara P, Xu Y, Liu X, Quaggin SE. Angiopoietin-1 knockout mice as a genetic model of open-angle glaucoma. Trans Vis Sci Tech. 2020;9(4):16, https://doi.org/10.1167/tvst.9.4.16

Purpose: A leading cause of blindness worldwide, glaucoma is often caused by elevated intraocular pressure (IOP) due to impaired aqueous humor outflow from the anterior chamber through Schlemm's canal (SC) and the trabecular meshwork. Despite the large clinical burden, glaucoma research and drug development are hindered by a limited selection of preclinical models that accurately recapitulate human disease. Here, we propose that *Angpt1* conditional knockout mice may provide one such model. Angiopoietin/TEK (ANGPT/TEK) signaling is crucial for SC formation and integrity in mice and humans, and mice lacking TEK or its ligand ANGPT1 develop a hypomorphic SC insufficient for normal aqueous humor outflow.

Methods: We used a comprehensive histology and physiology approach to characterize the glaucoma phenotype of *Angpt1* inducible knockout mice, especially focusing on retina morphology and function.

Results: *Angpt1* deletion resulted in persistent ocular hypertension beginning in the first month after birth and leading to decreased visual acuity with age due to glaucomatous neuropathy. In the neural retina, we identified marked and specific loss of the retinal ganglion cells, whereas other retinal neurons exhibited largely normal morphology and patterning. Electroretinogram recordings demonstrated reduced scotopic threshold response, further indicating loss of retinal ganglion cell function.

Conclusions: These findings highlight the potential of *Angpt1* conditional knockout mice as a valuable new glaucoma model.

Translational Relevance: Currently, few reliable, rapid-onset genetic glaucoma models are available, and *Angpt1* knockout mice will provide an additional tool for studies of IOP-induced neural damage, mechanisms of disease progression, and novel treatment strategies.

Introduction

Glaucoma is a devastating neurodegenerative disease that causes progressive, irreversible vision loss due to the death of retinal ganglion cells (RGCs). Elevated intraocular pressure (IOP) is the most important risk factor for glaucoma progression, and IOP reduction is the focus of current glaucoma therapy. Despite the effectiveness of IOP reduction for slowing disease progression, these treatments are not curative, nor can they restore lost vision or regenerate RGCs. Accordingly, research is ongoing to investigate other therapeutic approaches, including neuroprotection,

ganglion cell transplants, and new generations of IOP-lowering drugs.

Animal models that accurately recapitulate human disease provide an important resource for research on pathogenesis and drug design. Mouse models are especially valuable, as the low cost and rapid growth of mice make them ideal research subjects. Tools to study glaucoma-related phenotypes such as IOP, aqueous humor dynamics, visual acuity, RGC loss, and optic nerve morphology are widely available in mice, facilitating their use as a model system for this devastating disease.

We have recently described a key role for the angiopoietin (Angpt)-TEK endothelial receptor tyrosine kinase signaling pathway in IOP homeostasis.[1,2] In addition to the receptor tyrosine kinase TEK, this pathway includes the ligands ANGPT1, ANGPT2, and ANGPT4 and plays a key role in vascular and lymphatic development. Heterozygous loss of function mutations in TEK or its primary ligand ANGPT1 are associated with primary congenital glaucoma (PCG), a severe form of glaucoma characterized by early/childhood onset and optic neuropathy.[2,3] In addition to PCG, recent genome-wide association studies of subjects with adult-onset ocular hypertension or open-angle glaucoma have identified risk variants in the angiopoietin-TEK pathway, suggesting that defects in this signaling system may have a broader impact beyond PCG.[4–6] A likely mechanism for this ocular hypertension has been described in animal models, where mice lacking the TEK receptor fail to form Schlemm's canal (SC) and exhibit elevated IOP with a severe, glaucoma-like phenotype.[2] However, although *Tek* knockout animals rapidly develop optic neuropathy, interpretation is complicated, as TEK is essential for retinal angiogenesis.[7] In addition, we have noted the presence of kidney disease in *Tek* knockout animals—further complicating their use as an experimental model of glaucoma.[8]

The TEK ligand ANGPT1 is also essential for SC development. Mice lacking *Angpt1* after mid-gestation (*Angpt1*ΔWB mice) exhibit a hypomorphic SC that is insufficient for normal aqueous humor outflow, leading to ocular hypertension.[3] However, unlike *Tek* knockouts, these animals do not develop kidney disease and have a normal lifespan, due to compensation from the secondary ligand ANGPT2,[8,9] making them ideal for use as a highly clinically relevant genetic model of open-angle glaucoma. Here, we expand on our previous studies to describe the glaucoma phenotype of these animals in detail and provide a resource for other investigators interested in taking advantage of this new model of ocular hypertension and glaucoma.

Results

Angiopoietin-1 Knockout Mice Are a Genetic Model of High-Pressure Glaucoma

Angiopoietin-1 inducible knockout mice were generated using a doxycycline-based conditional gene deletion strategy to excise the first exon of *Angpt1* at embryonic day (E) 16.5. Resulting *Angpt1*ΔWB mice lack *Angpt1* expression in all tissues as previously described.[3,8,9] Lacking ANGPT1, *Angpt1*ΔWB mice develop a hypomorphic SC insufficient for normal aqueous humor drainage. IOP was measured weekly using rebound tonometry beginning at 3 weeks of age. Mutant animals rapidly developed ocular hypertension, reaching 20 mm Hg by 2 months of age (Fig. 1A). IOP elevation was bilateral, and at 3 months only a single animal (N = 25 *Angpt1*ΔWB mice) was recorded with unilateral ocular hypertension (Supplementary Figs. S1A, S1B). IOP elevation was observed in parallel colonies maintained at the Centers for Comparative Medicine of Northwestern University and the University of Virginia, confirming penetrance and reproducibility of the phenotype (Supplementary Fig. S1C). When measured using an optomotor response test (Fig. 1B, Supplementary Fig. S1D), progressive loss of visual acuity was observed in mutant mice. IOP remained elevated throughout life, and by 3 months of age increased axial length was observed in enucleated eyes from *Angpt1*ΔWB animals (Figs. 1C, 1D). Buphthalmos was apparent by 6 months (Fig. 1C).

To characterize the glaucomatous optic neuropathy observed in *Angpt1*ΔWB mice, retina flat mounts were prepared and RGCs were counted by immunofluorescent microscopy at 12 weeks of age (Figs. 2A–2C). We have previously noted that *Angpt1*ΔWB mice exhibit lower numbers of RGCs expressing both BRN3A (*Pou4f1*) and BRN3B (*Pou4f2*).3 However, this more detailed analysis revealed that RGC dropout was especially pronounced in the peripheral retina (BRN3A: central 14%, mid 18.7%, peripheral 32.6%; BRN3B: central 33.6%, mid 37%, peripheral 45%) (Figs. 2A, 2B). We additionally confirmed ganglion cell loss by staining for β-III-tubulin (TUBB3), a universal marker of RGCs. Although accurate counting of TUBB3+ RGCs was only possible in the peripheral retina due to TUBB3-positive nerve fibers obstructing visualization of cell bodies in the central retina, peripheral RGC loss was confirmed in *Angpt1*ΔWB eyes (control, 228.8 ± 14.9 TUBB3+ RGCs per 20× field; *Angpt1*ΔWB, 144.3 ± 21.1) (Fig. 2C). This

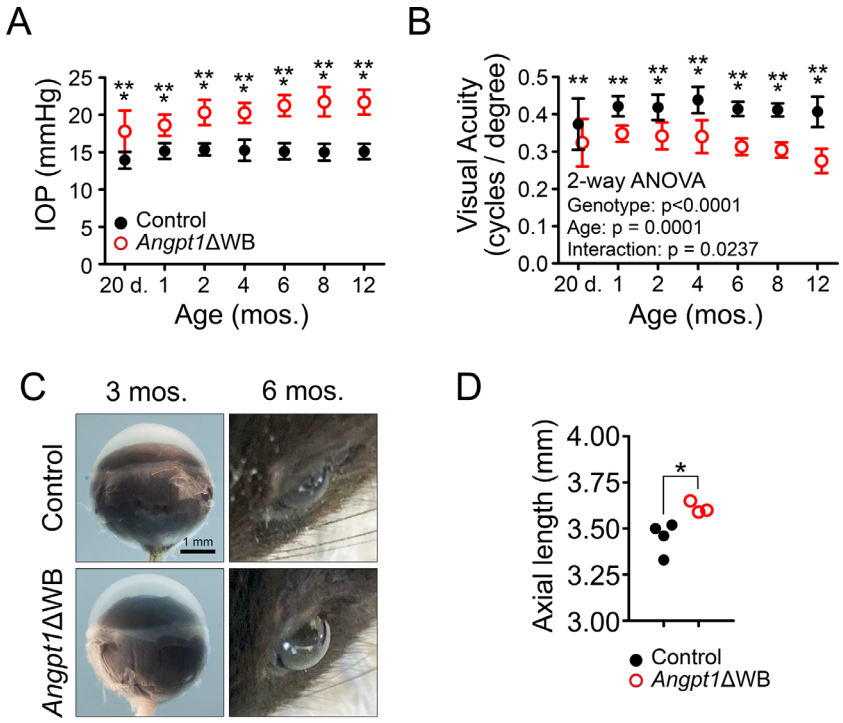

Figure 1. *Angpt1* knockout mice exhibit elevated IOP and vision loss. (A) Compared to controls, whole-body *Angpt1* knockout mice induced at mid gestation exhibit chronic IOP elevation when measured using rebound tonometry. Wild-type (WT): n = 34–54 (20 days to 4 months), n = 18 (6 months), and n = 12 (8–12 months); *Angpt1*ΔWB: n = 38–52 (20 days to 4 months), n = 24 (6 months), and n = 10 (8–12 months). (B) Similarly, progressive loss of visual acuity was detected in *Angpt1*ΔWB mice by optomotor response testing. WT: n = 25 (20 days), n = 9–14 (1–4 months), n = 21 (6 months), n = 8 (8 months), and n = 10 (12 months); *Angpt1*ΔWB: n = 10–15 (20 days to 2 months), n = 26 (4 months), and n = 8–10 (6–12 months). (C) Globe enlargement is apparent by 12 weeks of age, quantified in (D), and buphthalmos is visible at 6 months. *Scale bars*: 1 mm. $^{*}P < 0.05$, $^{**}P < 0.01$, $^{***}P < 0.001$, as determined by two-way ANOVA followed by Bonferroni's method for multiple comparisons (A, B) or Student's two-tailed *t*-test (D). Average axial length from each animal is plotted as a single data point in (D).

loss of TUBB3+ RGCs (37%) was consistent with the combined loss of BRN3A- and BRN3B-positive RGCs in the peripheral retina (36%), providing an internal control. RGC loss was not uniform throughout the retinal circumference, with local regions of higher RGC loss noted in the periphery of some animals, suggesting that individual nerve fiber bundles in the optic nerve head might be more susceptible to damage (Supplementary Fig. S2).

Additionally, to confirm our immunohistochemistry findings, we prepared optic nerve cross-sections from 6-month-old *Angpt1*ΔWB mice to analyze axon morphology. Compared to controls, marked axon loss (control, 45,920 ± 3513 axons; *Angpt1*ΔWB, 30,450 ± 2536 axons) (Fig. 3), and regions of gliosis were observed in mutant optic nerves. Importantly, the axon loss observed in *Angpt1*ΔWB mice (approximately 34%) was consistent with measurements obtained by quantification of TUBB3+ RGCs (36.8% loss of TUBB3+ RGCs) in retinal flat mounts.

Neuron Loss in *Angpt1* Knockout Retinas Is Specific to RGCs

As glaucoma is an RGC-specific neuropathy, we next examined other cell types in the retina to confirm the specificity of RGC loss in 3-month-old *Angpt1*ΔWB mice. Retina sections were prepared at the plane of the optic nerve head, and cell layers were quantified in the outer nuclear layer (ONL). Photoreceptor layers were counted in 4′,6-diamidino-2-phenylindole-stained sections in the central area, near the optic nerve, and in the peripheral region, near the retina edge. Compared to littermate control animals, no difference in ONL thickness was detected in *Angpt1*ΔWB mice (Fig. 4A, quantified in Fig. 4B). To specifically examine retina morphology in the inner nuclear layer (INL) and in the inner plexiform layer (IPL), we used additional antibodies against proteins expressed by cells in these strata (Fig. 4C): calbindin, present in horizontal cells and in their processes; a small number of amacrine cells of the INL; displaced

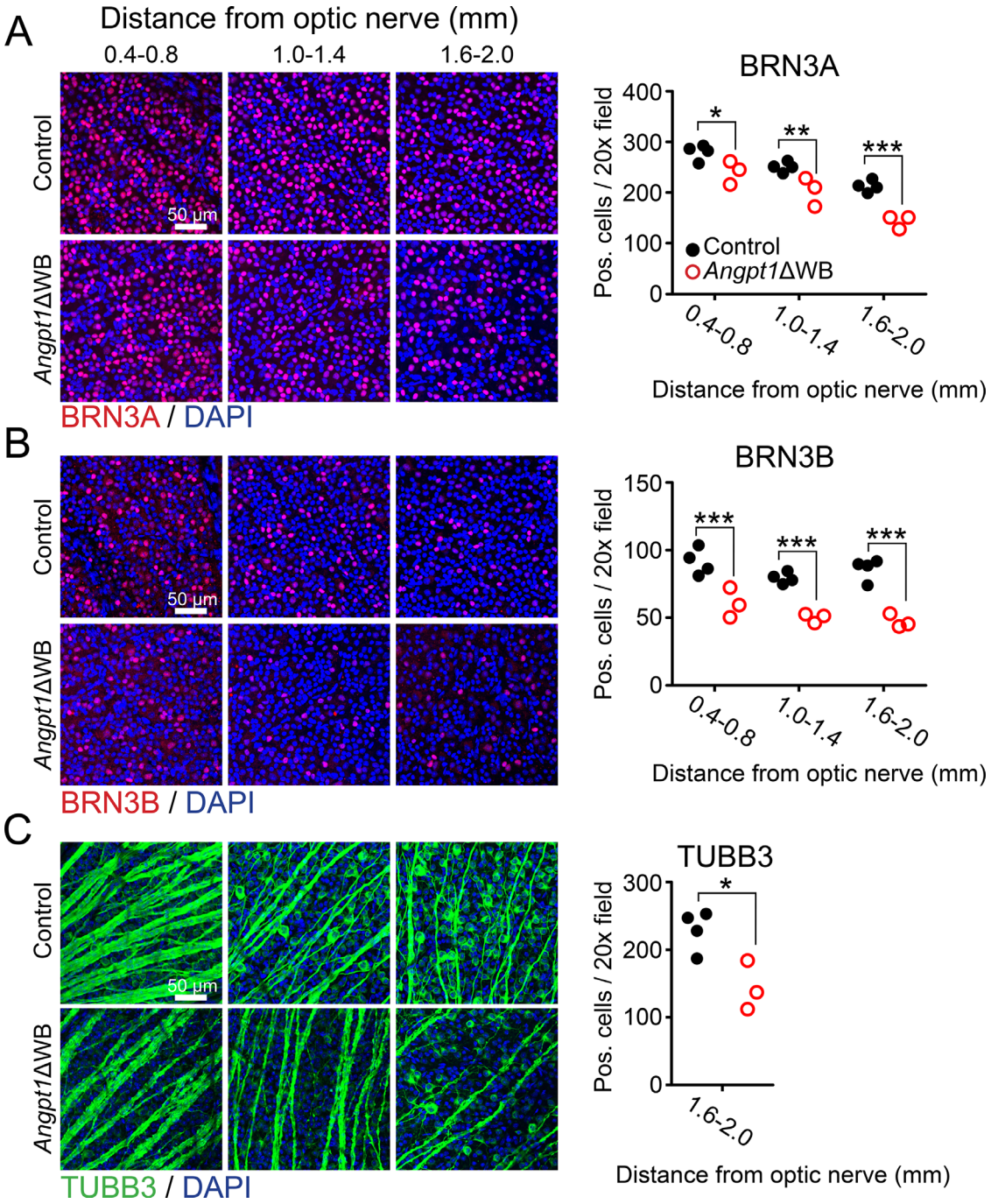

Figure 2. Retinal ganglion cell loss in *Angpt1* knockout mice. Compared to controls, 12-week-old *Angpt1*ΔWB mice exhibit reduced density of (A) BRN3A-, (B) BRN3B-, and (C) TUBB3-positive retinal ganglion cells when quantified in retina flat mounts. *Scale bars*: 50 μm; 20× fields represent an area of 65,413 μm^2. $^{*}P < 0.05$, $^{**}P < 0.01$, $^{***}P < 0.001$, as determined using two-way ANOVA followed by Bonferroni's method for multiple comparisons (A, B) or Student's two-tailed *t*-test (C). Average density obtained from each retina is shown as a single data point.

amacrine cells in the ganglion cell layer; some RGCs; and choline acetyltransferase, a marker of cholinergic amacrine cells, which also labels two narrow strata in the IPL. Calretinin labels amacrine cells, displaced amacrine cells, and some retinal ganglion cells. Three characteristic strata were labeled by calretinin in the IPL: the outer and the inner strata, representing the cholinergic strata, and the central band, which is comprised of putative bipolar axon terminals.[10] Antibodies against PROX1 strongly label amacrine and horizontal cell nuclei in the proximal and distal INL, and some bipolar cells are

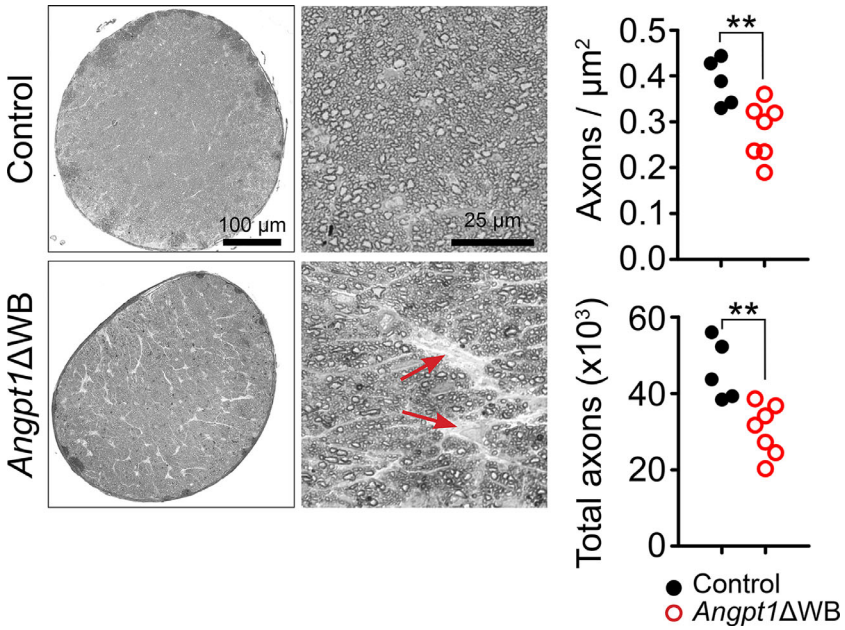

Figure 3. Optic nerve dysfunction in *Angpt1* knockout mice. Plastic sections (1-µm) stained with toluidine blue revealed reduced axon density and gliosis (red arrows) in 6-month-old mutant mice. $^{**}P < 0.01$ as determined by Student's two-tailed *t*-test. Each data point represents the average value obtained from a single animal.

also weakly immunostained. In addition, antibodies against protein kinase C-a (PKCα) were used to detect rod bipolar cells (Fig. 4D). PKCα stains both cell bodies and axon terminals of bipolar cells, which are located in the INL and IPL, respectively. Using this comprehensive panel of markers, no obvious changes were detected in the INL and IPL in *Angpt1*ΔWB mice.

To further evaluate functional changes in the retinas of *Angpt1*ΔWB mice, we conducted a series of electroretinogram (ERG) recordings. The initial waves of the scotopic (dark-adapted) ERG include the negative a-wave and positive b-wave and originate from cells at the early stages of retinal processing (Fig. 5A). Stimulated by a flash of light in darkness, the negative a-wave is generated by rod photocurrents before depolarizing bipolar cell currents then generate the positive b-wave (Fig. 5B). When measured at 4 to 6 months of age, *Angpt1*ΔWB mice exhibited a modest reduction in scotopic a-wave amplitude compared to controls only at higher levels of light stimulation (1–2 lg cd.s/m^2) (Figs. 5D–5F). A similar trend was observed in scotopic b-wave amplitude (Fig. 5E). Likewise, *Angpt1* deletion had little effect on a- or b-wave latency (time to peak amplitude), and increased latency was observed in mutant animals only at very low light intensity (–5 lg cd.s/m^2) (Fig. 5F). To test the light responses of cones, retina was light adapted for 10 minutes, and the photopic response was recorded. No obvious difference was noticed on photopic ERG across groups (data not shown). These results were consistent with our histological findings, suggesting that the outer retina was largely normal in *Angpt1*ΔWB mice at 4 to 6 months of age.

In addition to measuring a- and b-waves, we analyzed inner retina function by recording the scotopic threshold response (Fig. 5C) with a stimulation intensity of –4 lg cd.s/m^2. Amplitude of both positive (pSTR) and negative (nSTR) components of the scotopic threshold response were found to decrease with age in *Angpt1*ΔWB mice (Figs. 5D, 5G, 5I), further confirming progressive RGC loss in these animals. Latency of both positive and negative STR was unaffected in mutant mice (Figs. 5H, 5J).

Angpt1 Knockout Mice Have Normal Retinal Vasculature

The ocular hypertension, decreased visual acuity, and specific RGC loss observed in *Angpt1*ΔWB mice were consistent with high-pressure glaucomatous optic neuropathy. However, *Angpt1* is a vascular growth factor, and to rule out the possibility that RGC loss is due to vascular defects and retinal ischemia we examined the retinal vasculature of *Angpt1*ΔWB mice in detail. Unlike *Angpt2* or *Tek* knockout mice, which

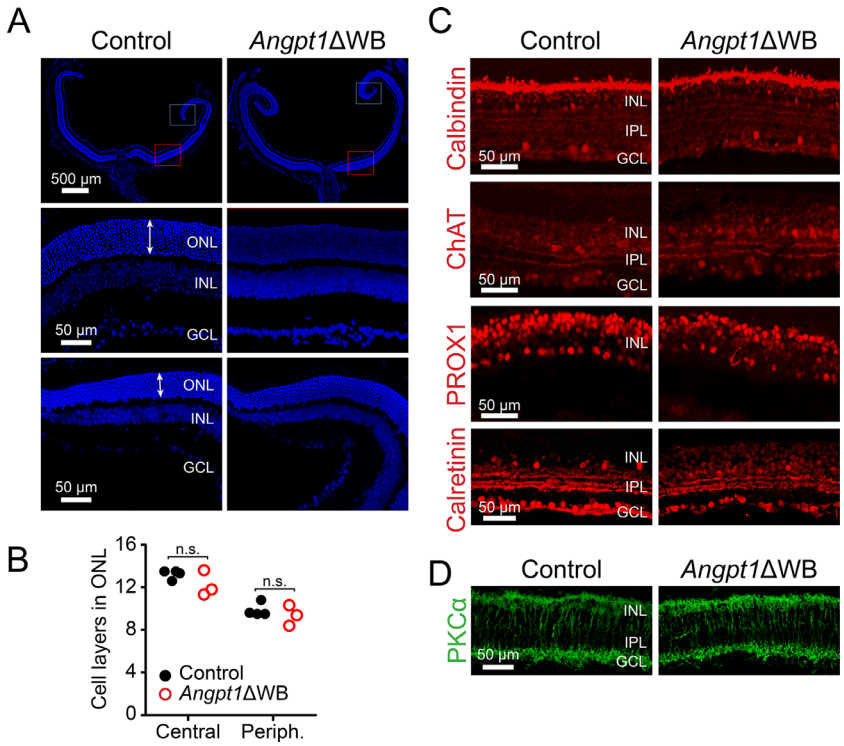

Figure 4. *Angpt1* knockout retinas have normal morphology. (A, B) The 4′,6-diamidino-2-phenylindole-stained cryosections from 12-week-old mice show normal retinal morphology, with no significant difference in ONL thickness between control and *Angpt1*ΔWB mice in either central (red squares) or peripheral (blue squares) retina (control n = 14, *Angpt1*ΔWB n = 14; $P = 0.8$). (C) Calbindin, choline acetyltransferase (ChAT), PROX1, and calretinin show no difference in horizontal or amacrine cell morphology in *Angpt1*ΔWB mice. (D) Likewise, no changes in PKCα-stained rod bipolar cells were observed. *Scale bars*: 500 μm and 50 μm (A) and 50 μm (C, D). Not significant $P > 0.05$ as determined by two-way ANOVA followed by Bonferroni's method for multiple comparisons.

exhibit severely reduced retinal angiogenesis, developmental angiogenesis of the superficial vascular plexus was normal in *Angpt1*ΔWB mice when imaged at P5 (Fig. 6A). In adults, in vivo fundus microscopy revealed no apparent vascular defects in the retinas of *Angpt1*ΔWB animals at 3 months of age (Fig. 6B). To confirm this finding, retinas were collected and flat mounts were examined using confocal microscopy. Using this technique, we observed normal patterning and vascular area in the superficial vascular layer, which supplies the RGCs. (Fig. 6C). Likewise, normal patterning was observed in the intermediate and deep vascular layers of *Angpt1*ΔWB mice (Fig. 6D).

Methods

Animal Generation and Husbandry

Mice were housed at the Centers for Comparative Medicine of Northwestern University (Chicago, IL, USA), and the University of Virginia (Charlottesville, VA, USA). Whole-body *Angpt1* knockout mice were generated and induced with doxycycline-containing drinking water as previously described.[3,9] Briefly, timed matings were conducted and pregnant females were switched from plain water to doxycycline-containing water (0.5% in 5% sucrose) to trigger gene deletion at E16.5. Dams and neonates were allowed ad libitum access to doxycycline-containing water until P14. *Angpt1*$^{flox/flox}$;TetOnCre+ littermates lacking the reverse tetracycline-controlled transactivator (rtTA) transgene are protected from doxycycline-mediated Cre recombinase expression and were used as controls throughout the study. Animals were given unrestricted access to standard rodent chow and water (or doxycycline-containing water) and maintained on a standard 12-hour light cycle. All mice were kept on a mixed genetic background free of the RD1 and RD8 mutations, and animals of both sexes were included in all comparisons. Knockout mice were genotyped by PCR as previously described,[3] with rtTA-negative littermates being used as controls. Animals were included in the study on a "by-litter" basis, and mutant mice were never included without their matching littermate controls.

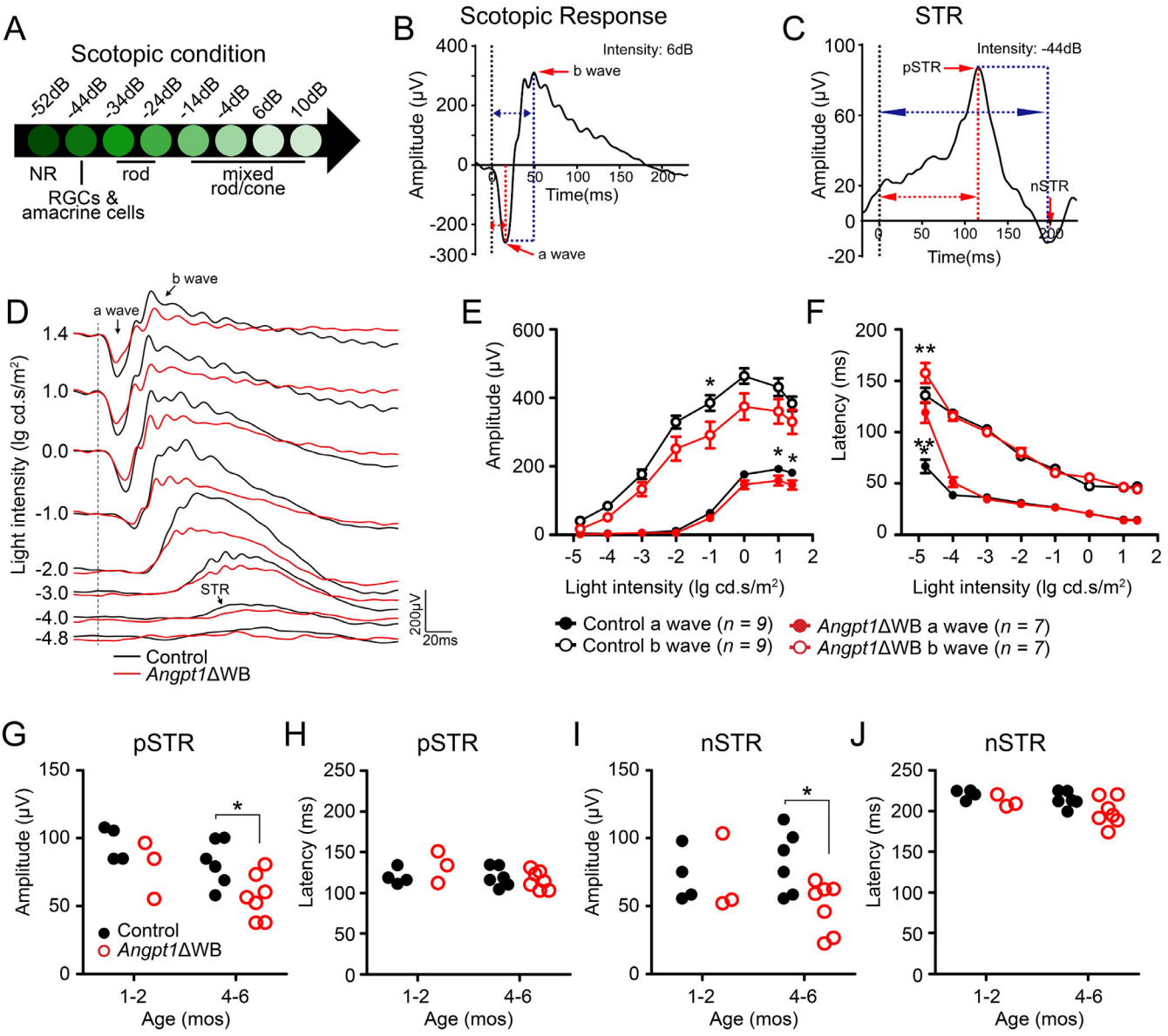

Figure 5. Scotopic ERG response in *Angpt1* knockout mice. (A) Representation of light stimulation in scotopic recording. Before stimulation, mice were dark adapted for 12 hours to maximize retinal sensitivity. (B) Example waveform for scotopic response. The negative a-wave is mainly derived from rods, and the b-wave is a positive-going potential primarily derived from bipolar cells. (C) The STR waveform consists of pSTR and nSTR components that represent RGCs and AII amacrine cells, respectively. (D) Examples of scotopic ERG response traces from control and *Angpt1*ΔWB mice in response to flash intensities ranging from –4.8 to 1.4 lg cd·s/m^2 (–52 to 10 dB). (E) Intensity response curves from 4- to 6-month-old control and *Angpt1* knockout mice. Compared to controls, mutant animals exhibited similar a- and b-wave amplitudes with only a slight reduction observed at high flash intensity (control n = 9, *Angpt1*ΔWB n = 7). (F) Latency of a- and b-waves was largely unchanged in *Angpt1*ΔWB mice. (G) Scotopic threshold measurements recorded at –4 lg cd·s/m^2 in control and *Angpt1*ΔWB mice revealed an age-related loss of RGC-derived positive current (pSTR) in mutant animals (control, 1–2 months, n = 4; control, 4–6 months, n = 6; *Angpt1*ΔWB, 1–2 months, n = 3; *Angpt1*ΔWB, 4–6 months, n = 7). (H, J) The response latency was unchanged. (I) A similar age-related loss of nSTR was observed in mutant animals. (J) nSTR latency was unchanged. $^{*}P < 0.05$, $^{**}P < 0.01$ as determined by two-way ANOVA followed by Bonferroni's method for multiple comparisons. Horizontal arrows in (B) and (C) indicate latency measurements.

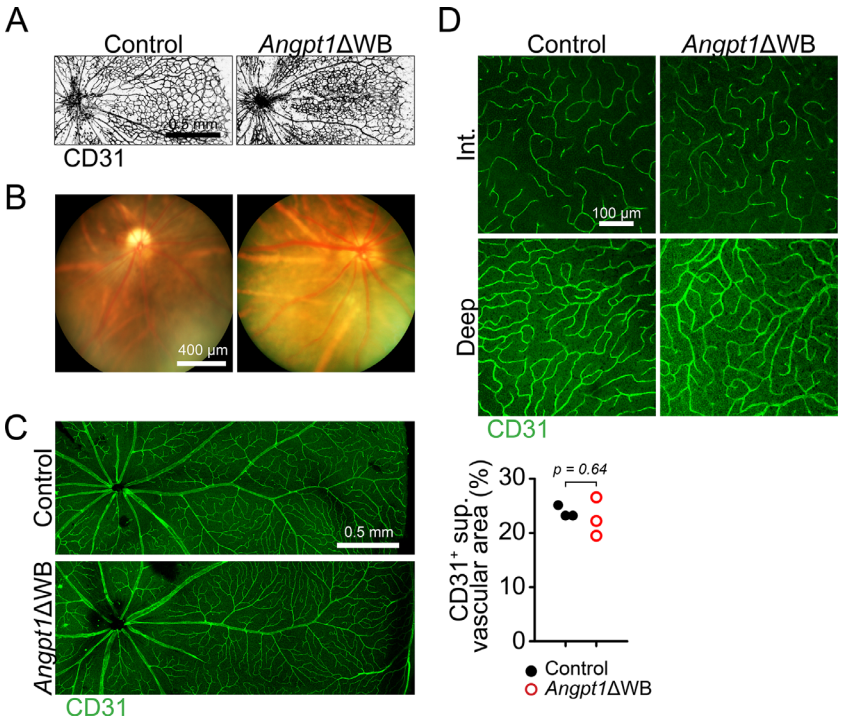

Figure 6. *Angpt1* knockout mice have normal retinal vasculature. (A) Retinal flat mounts of P5 mice reveal normal angiogenesis and sprouting front progression in Angpt1 knockout retinas. (B) In adult eyes, color fundus microscopy revealed normal vascular patterning in *Angpt1*ΔWB mice at 3 months of age. (C) This finding was confirmed in retinal flat mounts, where no differences in vascular patterning or CD31-positive (pos.) area were observed in the superficial (sup.) layer of *Angpt1*ΔWB retinas. (D) Likewise, normal patterning was observed in the intermediate (int.) and deep vascular layers. *Scale bars*: 500 µm (A, C), 400 µm (B), and 100 µm (D). Lack of significance in (B) was confirmed using a two-tailed Student's *t*-test.

Intraocular Pressure Measurements

IOP was measured in awake mice using a Tonolab rebound tonometer (iCare, Raleigh, NC, USA) as previously described.[1,11] Animals were restrained in a soft plastic cone, and IOP values were obtained as averages from three sets of six recordings on each eye performed by a blinded technician.[10,12] Each mouse was measured under ambient lighting between 9:30 AM and 11:00 AM on 2 subsequent days, and the results were averaged to obtain reported values. Finding a strong correlation between left and right eyes (Supplementary Fig. S1A) and no difference between left and right eyes using a paired *t*-test (Supplementary Fig. S1B) (control: Δ0.37 mm Hg, $P = 0.25$; *Angpt1*ΔWB: Δ–0.38 mm Hg, $P = 0.17$), we have reported all IOP measurements as a single averaged value for each animal.

Optomotor Response Test

Visual acuity was quantified using an optomotor response test (PhenoSys qOMR, PhenoSys GmbH, Berlin, Germany). Mice were placed on an elevated central platform surrounded by four monitors to evoke an optokinetic response and top and bottom mirrors to create the illusion of infinite depth. After 1 minute of adaptation with gray screen, vertical black and white stripes of a defined spatial frequency moving horizontally were presented to the animal. These stripes were rotated alternately clockwise and anticlockwise for 10 seconds in each direction. We tested 200 mice (90 control; 110 *Angpt1*ΔWB) with various spatial frequencies from 0.00 to 0.50 cycles/deg. Mouse visual acuity was measured biweekly from 1 to 52 weeks of age by two persons independently. Animals were videotaped with an infrared camera and re-examined for confirmation when needed. As visual acuity increases in wild-type mice between P20 and 1 month of age,[13] the P20 time point was excluded when performing regression analysis to allow rational fitting of a linear model.

In Vivo Imaging

Three-month-old mice were anesthetized with intraperitoneal ketamine (100 mg/kg; Henry Schein, Melville, NY, USA) and xylazine (10 mg/kg; Henry Schein), and eyes were dilated with 1% tropicamide ophthalmic solution (NDC #17478-102-12; Akorn

Inc., Lake Forest, IL, USA). Images were taken using a Micron IV retinal imaging system (Phoenix Research Laboratories, Pleasenton, CA, USA). After in vivo imaging, some animals were allowed to recover on a heating pad, and others were intracardially perfused and eyes enucleated for histological analysis.[14,15] After recovery, animals were allowed to rest for at least 1 week before undergoing visual acuity and IOP measurement.

RGC Quantification

*Angpt1*ΔWB mice and control littermates were anesthetized (ketamine/xylasine; Henry Schein) and perfusion fixed (2% formaldehyde in 0.1-M $NaHP0_4$, pH 7.5). After perfusion, samples were immersion fixed for an additional 12 hours. Retinas were collected and blocked (5% donkey serum, 2.5% bovine serum albumin, 0.5% Triton X-100 [Sigma-Aldrich, St. Louis, MO, USA] in Tris-buffered saline, pH 7.5, overnight at 4°C) before overnight incubation with appropriate primary and Alexa Fluor-labeled secondary antibodies (ThermoFisher Scientific, Waltham, MA, USA). Stained retinas were flat mounted and imaged using a Nikon A1R confocal microscope (Tokyo, Japan) equipped with a 20× objective with a numeric aperture of 0.75 and a pinhole size of 44.70 µm. This configuration resulted in a field area of 65,413 μm^2. The retina was divided into three imaging zones based on distance from the optic nerve head: central (0.4–0.8 mm), mid (1.0–1.40), and peripheral (1.6–2.0). Four images were captured at intervals around the retinal circumference in each zone (Supplementary Fig. S2A), and positive cells were counted using ImageJ software.[16] Cell counts per field were averaged to obtain the values reported in the manuscript. Primary antibodies used included mouse anti-BRN3A (MAB1585, 1:400; Millipore, Burlington, MA, USA), goat anti-BRN3B (sc-6026, 1:400; Santa Cruz Biotechnology, Dallas, TX, USA), and rabbit anti-TUBB3 (MRB-435P, 1:1000; Covance, Princeton, NJ).

Optic Nerve Morphology

After perfusion with 2% formaldehyde as above, optic nerves were collected and post fixed (2% glutaraldehyde, 4% formaldehyde in 0.1-M sodium cacodylate, pH 7.2). Nerves were then embedded in EPON resin (Hexion, Columbus, OH, USA), and 1-µm sections were prepared and stained with toluidine blue. Brightfield images were captured using a Nikon Ti2 microscope equipped with a DS-Qi2 camera and 40× objective with a numeric aperture of 1.3. Images were captured at a resolution of 0.12 µm/pixel. For quantification, a 100 × 100-pixel grid was overlaid on the optic nerve image using Fiji software, and axons were counted in every sixth grid square, resulting in 14 to 16 counted regions per nerve. Values were averaged to obtain axon counts reported in the manuscript and multiplied by cross-sectional area to estimate total axon number.

Immunohistochemistry

For paraffin sections, eyes were fixed as above before embedding in paraffin using a Leica TP1020 tissue processor (Wetzlar, Germany). Then, 5-µm sections were prepared and subjected to antigen retrieval (10-mM Tris, 1-mM ethylenediaminetetraacetic acid containing 0.05% Tween 20 [Sigma-Aldrich], pH 9.0, autoclaved on liquid cycle, 30-minute sterilization time). Blocking and staining were as above. For cryosections, eye cups were fixed, cryoprotected in 30% sucrose solution overnight, embedded in OCT medium (Sakura Finetek, Torrance, CA, USA), and sectioned by cryostat at 12 to 16 µm. Retina sections were blocked and stained as above. Primary antibodies used included rat anti-CD31 (#553370, 1:100; BD Biosciences, Franklin Lakes, NJ, USA), rabbit anti-calbindin (Chemicon, #AB2724, 1:1000; Sigma-Aldrich), rabbit anti-choline acetyltransferase (#PA5-29653, 1:500; ThermoFisher Scientific), goat anti-PROX1 (#AF2727, 1:500; R&D Systems, Minneapolis, MN, USA), rabbit anti-calretinin (Chemicon, #AB5054; 1:1000; Sigma-Aldrich), and mouse anti-PKCα (NB600-201, 1:500; Novus Biologicals, Centennial, CO, USA). After several washes, secondary antibodies were applied for 2 hours at room temperature. These included donkey anti-mouse immunoglobulin G (IgG) conjugated to Alexa Fluor 488 dye (green fluorescence) and donkey anti-rabbit IgG and donkey anti-rat IgG either conjugated to Alexa Fluor 594 dye (red fluorescence) (ThermoFisher Scientific), all diluted 1:1000. Three-dimensional Z stacks were captured on a Carl Zeiss LSM 800 microscope (Oberkochen, Germany) and subsequently projected to a two-dimensional plane.

Analysis of Retinal Vascular Patterning

Retinal flat mounts were prepared as described above, before overnight incubation with rat anti-CD31 (#553370, 1:100; BD Biosciences) primary antibody. Retinas were then washed, incubated with appropriate secondary antibodies, and mounted on slides for microscopic analysis. Images of the superficial vasculature were captured on a Nikon A1R confocal microscope equipped with a 10× objective (numerical aperture, 0.3;

pinhole, 1.2 Airy units) and stitched to obtain views of the full flat-mounted retinas. CD31-positive superficial vascular area was then quantified using AngioTool software.[17] Images of the intermediate and deep vascular layers were captured using a 20× objective (numerical aperture, 0.75; pinhole, 1.2 Airy units).

Full-Field ERG Recordings

ERG recordings were performed using the UTAS Visual Diagnostic Test System (LKC Technologies, Gaithersburg, MD, USA) according to published procedures.[12] In brief, mice were dark adapted overnight before recording, and all the procedures were performed under dim red light. Mice were anesthetized with ketamine/xylazine solution (100–20 mg/ml). The pupils were dilated by 1% tropicamide (Akorn) and 2.5% phenylephrine (Bausch & Lomb, Tampa, FL, USA). Gonak hypromellose 2.5% solution (Akorn) was used to maintain corneal hydration, and a gold-plated electrode was placed in contact with the cornea for ERG recordings. Stainless steel electrodes were inserted into the skin near the eye as the reference electrode and into the tail as the ground electrode. Mice were placed on a heated platform, and data were collected using a LKC Technologies amplifier system at a 2-kHz sampling rate. After 2- to 3-hour sessions, animals were recovered from anesthesia on a heating pad.

Full-field ERGs were obtained with flashing white light at different intensities (from –4.8 to 1.4 lg cd·s/m^2 or –52 to 10 dB). Flash stimuli below 1.4 lg cd·s/m^2 were delivered by green light-emitting diode (530 nm, highest luminance 2.2 lg cd·s/m^2). Each scotopic condition represents the average of 10 flash stimuli responses. The interval between the stimuli was 5 seconds at low intensities and 10 seconds at intensities above 0 lg cd·s/m^2. Scotopic threshold responses (STRs) were obtained at an intensity of –4 lg cd·s/m^2. Scotopic stimuli were converted to photoisomerizations/rod unit, where 1 scot cd/m^2 was equal to 581 photoisomerizations/rod. This intensity was chosen to obtain reliable STR measurements independent from the b-wave.[18,19] The electrical signals from the retinas were analyzed with Axon Clampfit software (Molecular Devices, San Jose, CA, USA) after applying a 50-Hz low-pass filter with Gaussian smoothing to remove oscillatory potentials as previously described.[20–22] The a-wave amplitude was measured from baseline to the first negative peak, and the b-wave amplitude was measured from the a-wave trough to the subsequent positive peak. A digital 60-Hz notch filter and Gaussian smoothing filter were used to graph positive and negative STRs. Note that the 50-Hz low-pass filter slightly distorted the high-frequency components in the rising phase of the a-wave, resulting in a reduced amplitude (up to 10% at 1.0 lg cd·s/m^2) and a shorter time-to-peak of the a-wave than raw data (up to 7% at 1.0 lg cd·s/m^2). The same filter was applied for all intensities and experimental groups, and the extent of the distortion on the a-wave was similar between control and *Angpt1*ΔWB mice. Because we found no difference in a- or b-wave amplitude and latency in either control or *Angpt1*ΔWB mice between 4 and 6 months of age, animals from these age groups were pooled for analysis.

Study Approval

All animal experiments were approved by the Animal Care and Use Committees at the Centers for Comparative Medicine of Northwestern University and the University of Virginia and comply with ARVO guidelines for care and use of vertebrate research subjects.

Statistical Analysis

Analysis was performed using Prism 5 software (GraphPad Software, San Diego, CA, USA). Throughout the text, values are reported as mean ± standard error of the mean. Indicated P values were obtained using a two-tailed Student's t-test, one-way analysis of variance (ANOVA) followed by the Tukey–Kramer test, or two-way ANOVA followed by use of Bonferroni's method for multiple comparisons. Comparison among regression-fitted slopes was conducted using GraphPad Prism 5 software and a method equivalent to analysis of covariance (ANCOVA). Tests used for specific data are noted in the figure legends. $P < 0.05$ was considered significant, as indicated by the following notation: $^{*}P < 0.05$, $^{**}P < 0.01$, $^{***}P < 0.001$.

Discussion

Rodent models have been widely used in glaucoma research and have provided invaluable insights into the pathogenesis, genetics, and treatment of human disease. A complete discussion of all available models is beyond the scope of this manuscript (and has been the subject of excellent recent reviews, including Fernandes et al.[23] and Johnson et al.[24]), but contextualizing our results in relation to some existing models will aid in evaluating the utility of *Angpt1*ΔWB mice in the study of glaucoma.

Several genetic models of ocular hypertension, glaucoma, and anterior segment dysgenesis have been described. Of these, the most widely used are the DBA/2J inbred mouse strain. DBA/2J mice develop elevated IOP due to iris pigment dispersion and stromal atrophy caused by mutations in *Gpnmb* and *Tyrp1*, which are believed to result in a defective innate immune response.[25–27] IOP elevation in DBA/2J mice occurs between 8 and 12 months of age, and pressure can be as high as 30 to 40 mm Hg in some animals.[25] Although timing and penetrance are variable, approximately 50% of mutant eyes have optic nerve damage by 10 months. The variable penetrance and late onset of disease complicate studies using the DBA/2J model, as large numbers of animals must be kept and aged for several months.[28] Despite these challenges and the profound mechanistic differences from human disease, research with DBA/2J mice has provided many valuable insights into glaucoma pathogenesis, treatment, and prevention; however, there is an unmet need for new genetic models that are more consistent with a faster onset or more closely mimic human disease.

*Angpt1*ΔWB Mice Are a Model of High-Pressure Open-Angle Glaucoma

Due to defects in SC development and function,[3] *Angpt1*ΔWB mice develop ocular hypertension by 3 weeks, reaching 20 mm Hg between 6 and 8 weeks of age and stabilizing at 20 to 22 mm Hg. This increase of 5 to 6 mm Hg compared to controls was comparable to that observed in patients with primary open-angle glaucoma.[29] The time course observed was shorter than that reported in DBA/2J mice, facilitating shorter experimental timelines. In addition, ocular hypertension in *Angpt1*ΔWB mice has a very high penetrance, even when maintained on a mixed genetic background as in the current study. At 12 weeks of age, 67% of *Angpt1*ΔWB mice examined had an IOP $>$ 5 mm Hg higher than the average pressure of matching controls. Furthermore, unlike DBA/2J mice, IOP elevation in *Angpt1*ΔWB mice was bilateral, and only a single animal was observed with unilateral hypertension at 12 weeks of age. This correlation between left and right eyes allows experimental use of both eyes and further reduces the animal numbers required for experimental studies, allowing researchers either to subject each globe to different histological preparation (as here) or to use an untreated contralateral eye as an experimental control in interventional studies.

Elevated IOP is the primary glaucoma risk factor, and IOP lowering is frequently used as the primary endpoint in clinical trials.[30] Many eyes with elevated IOP, however, do not develop glaucomatous optic neuropathy,[31] necessitating a careful analysis of new glaucoma models. We have previously reported that loss of BRN3-positive RGCs occurs in *Angpt1* knockout mice, suggesting that these animals are a model of high-pressure glaucoma.[3] However, it has been reported that RGCs may lose BRN3A expression prior to apoptosis, potentially leading to overestimation of RGC dropout in glaucoma and necessitating comparison to other RGC markers and histological readouts.[32] Here, we expanded on our previous analysis by performing zone-specific quantification of RGC loss in *Angpt1*ΔWB mice. We also confirmed a robust correlation between loss of RGCs stained with BRN3A/B and TUBB3, a neural tubulin highly expressed by RGCs.[33] In 3-month-old *Angpt1*ΔWB mice, loss of BRN3A- and BRN3B-expressing RGCs was apparent, with the most severe loss (BRN3A, 33%; BRN3B, 45%) localized in the peripheral retina. Although only a single time point was measured in our study, the pattern we observed was similar to but more severe than that described in hypertensive mice expressing the glaucoma mutant Y437H human *MYOC* which exhibit a 20% loss of peripheral RGCs by 18 months of age.[34] Although immunostaining of retinal ganglion cell somas has been widely validated for analysis of RGC loss in glaucoma, direct analysis of RGCs by dye backfilling or histological analysis of optic nerve axons remains the most robust method of observing RGC dropout. Loss of RGC axons has been well described in animal models of high-IOP glaucomatous neuropathy including DBA/2J, *MYOC* mutants, and laser photocoagulation.[10,25,34] Importantly, optic nerve histology of *Angpt1*ΔWB mice confirmed the RGC loss we observed by immunostaining, precluding the possibility that loss of specific molecular markers could account for the apparent decrease in RGC numbers observed in mutant mice. Importantly, RGC loss in *Angpt1* knockout mice is specific and other retinal neurons appear to be minimally functionally or morphologically affected.

In addition to IOP elevation, retinal perfusion deficits can also lead to RGC death, complicating analysis of glaucoma models involving endothelial signaling pathways. Acute ischemic injury leads to rapid ganglion cell loss in animal models,[35] and low or unstable ocular perfusion pressure has been linked with disease progression patients.[36,37] In addition to its role in SC, TEK signaling plays a key role in retinal angiogenesis, although the role of ANGPT1 is poorly described.[38,39] Outside of the eye, *Angpt1* knockout mice have defects in vascular remodeling,[9] and ANGPT1 overexpression leads to dermal

capillary widening.[40,41] In the retina, *Angpt1* is expressed by neurons adjacent to the superficial and intermediate vascular layers, although not in RGCs.[42,43] It has been reported that whole-body, inducible *Angpt1* knockout mice deleted at E13.5 have normal retinal angiogenesis when imaged at P9.[9] Importantly, our data support this finding, indicating that *Angpt1* is not required for retinal angiogenesis and suggesting that RGC loss in *Angpt1*ΔWB mice is likely due to IOP elevation rather than retinal ischemia.

Insufficient aqueous humor outflow through the conventional route is thought to be the leading cause of ocular hypertension in glaucoma patients. Just as the conventional route is responsible for the majority of aqueous humor outflow, it is similarly important in many small animal glaucoma models, including laser photocoagulation, microbead injection, and DBA/2J mice, all of which are thought to reduce outflow through SC and the trabecular meshwork.[25,44,45] Disruption of the conventional outflow is a clinically relevant strategy for modeling the effect of IOP elevation on the retina but complicates the use of these models for testing SC- and trabecular meshwork-specific glaucoma therapies. Exhibiting a hypomorphic SC, we hypothesize that IOP elevation in *Angpt1*ΔWB is similarly due to reduced conventional outflow; however, we have previously reported that IOP in these animals is significantly lower than that observed in *Angpt1*;*Angpt2* double knockout mice, which completely lack SC, suggesting that some outflow through the conventional route remains.[3] Therefore, it is possible that that SC or trabecular meshwork targeting therapies may be effective in these animals, although further studies would be required to ascertain the usefulness of the model in this area.

Taken together, our data indicate that *Angpt1*ΔWB mice reliably develop bilateral ocular hypertension, buphthalmos, and glaucomatous optic neuropathy, likely due to insufficient aqueous humor outflow provided by a hypomorphic SC. As *Angpt1* mutations have also been identified in human patients, our data suggest that *Angpt1*ΔWB mice may provide a valuable, clinically relevant model of PCG.

Acknowledgments

We thank Harry A. Quigley and Mary Ellen Pease for scientific input and Megan Kelly for technical assistance. Lennell Reynolds, Jr., performed histology of optic nerves.

This study was funded by NIH R01 HL124120, R01 EY025799 (SEQ), and R01EY029121 (XL). FL was supported by the 111 Project, Ministry of Education and State Administration of Foreign Experts Affairs of PRC (B14036) and the Lin Jian Biomedicine Development Foundation of Jinan University. Imaging was performed at the Northwestern University Center for Advanced Microscopy supported by NCI CCSG P30 CA060553 awarded to the Robert H. Lurie Comprehensive Cancer Center. We also acknowledge support from George M. O'Brien Kidney Core Grant P30 DK114857.

Disclosure: **B.R. Thomson**, None; **M. Grannonico**, None; **F. Liu**, None; **M. Liu**, None; **P. Mendapara**, None; **Y. Xu**, None; **X. Liu**, None; **S.E. Quaggin**, Mannin Research, Inc. (F, I, E), therapeutic targeting of the ANGPT-TEK pathway in ocular hypertension and glaucoma (P)

* BRT and MG contributed equally to this article.

References

1. Thomson BR, Heinen S, Jeansson M, et al. A lymphatic defect causes ocular hypertension and glaucoma in mice. *J Clin Invest*. 2014;124:4320–4324.
2. Souma T, Tompson SW, Thomson BR, et al. Angiopoietin receptor TEK mutations underlie primary congenital glaucoma with variable expressivity. *J Clin Invest*. 2016;126:2575–2587.
3. Thomson BR, Souma T, Tompson SW, et al. Angiopoietin-1 is required for Schlemm's canal development in mice and humans. *J Clin Invest*. 2017;127:4421–4436.
4. Khawaja AP, Cooke Bailey JN, Wareham NJ, et al. Genome-wide analyses identify 68 new loci associated with intraocular pressure and improve risk prediction for primary open-angle glaucoma. *Nat Genet*. 2018;50:778–782.
5. Gao XR, Huang H, Nannini DR, Fan F, Kim H. Genome-wide association analyses identify new loci influencing intraocular pressure. *Hum Mol Genet*. 2018;27:2205–2213.
6. MacGregor S, Ong J-S, An J, et al. Genome-wide association study of intraocular pressure uncovers new pathways to glaucoma. *Nat Genet*. 2018;50:1067–1071.
7. Chu M, Li T, Shen B, et al. Angiopoietin receptor Tie2 is required for vein specification and maintenance via regulating COUP-TFII. *eLife*. 2016;5:e21032.

8. Kenig-Kozlovsky Y, Scott RP, Onay T, et al. Ascending vasa recta are angiopoietin/Tie2-dependent lymphatic-like vessels. *J Am Soc Nephrol*. 2017;29:1097–1107.
9. Jeansson M, Gawlik A, Anderson G, et al. Angiopoietin-1 is essential in mouse vasculature during development and in response to injury. *J Clin Invest*. 2011;121:2278–2289.
10. Feng L, Zhao Y, Yoshida M, et al. Sustained ocular hypertension induces dendritic degeneration of mouse retinal ganglion cells that depends on cell type and location. *Invest Ophthalmol Vis Sci*. 2013;54:1106–1117.
11. John SW, Hagaman JR, MacTaggart TE, Peng L, Smithes O. Intraocular pressure in inbred mouse strains. *Invest Ophthalmol Vis Sci*. 1997;38:249–253.
12. Chen H, Zhao Y, Liu M, et al. Progressive degeneration of retinal and superior collicular functions in mice with sustained ocular hypertensiondegeneration of visual functions in glaucoma. *Invest Ophthalmol Vis Sci*. 2015;56:1971–1984.
13. Prusky GT, Alam NM, Beekman S, Douglas RM. Rapid quantification of adult and developing mouse spatial vision using a virtual optomotor system. *Invest Ophthalmol Vis Sci*. 2004;45:4611–4616.
14. Puyang Z, Feng L, Chen H, Liang P, Troy JB, Liu X. Retinal ganglion cell loss is delayed following optic nerve crush in NLRP3 knockout mice. *Sci Rep*. 2016;6:20998.
15. Feng L, Puyang Z, Chen H, Liang P, Troy JB, Liu X. Overexpression of brain-derived neurotrophic factor protects large retinal ganglion cells after optic nerve crush in mice. *eNeuro*. 2017;4:0331–0316.2016.
16. Schindelin J, Arganda-Carreras I, Frise E, et al. Fiji: an open-source platform for biological-image analysis. *Nat Meth*. 2012;9:676–682.
17. Zudaire E, Gambardella L, Kurcz C, Vermeren S. A computational tool for quantitative analysis of vascular networks. *PLoS One*. 2011;6:e27385.
18. Frankfort BJ, Khan AK, Tse DY, et al. Elevated intraocular pressure causes inner retinal dysfunction before cell loss in a mouse model of experimental glaucoma. *Invest Ophthalmol Vis Sci*. 2013;54:762–770.
19. Saszik SM, Robson JG, Frishman LJ. The scotopic threshold response of the dark-adapted electroretinogram of the mouse. *J Physiol*. 2002;543:899–916.
20. Lei B, Yao G, Zhang K, Hofeldt KJ, Chang B. Study of rod- and cone-driven oscillatory potentials in mice. *Invest Ophthalmol Vis Sci*. 2006;47:2732–2738.
21. Smith BJ, Tremblay F, Côté PD. Voltage-gated sodium channels contribute to the b-wave of the rodent electroretinogram by mediating input to rod bipolar cell GABAc receptors. *Exp Eye Res*. 2013;116:279–290.
22. Yang S, Luo X, Xiong G, So K-F, Yang H, Xu Y. The electroretinogram of Mongolian gerbil (*Meriones unguiculatus*): comparison to mouse. *Neurosci Lett*. 2015;589:7–12.
23. Fernandes KA, Harder JM, Williams PA, et al. Using genetic mouse models to gain insight into glaucoma: past results and future possibilities. *Exp Eye Res*. 2015;141:42–56.
24. Johnson TV, Tomarev SI. Animal models of glaucoma. In: Chan C-C, ed. *Animal Models of Ophthalmic Diseases*. Cham, Switzerland: Springer; 2016:31–50.
25. Libby RT, Anderson MG, Pang I-H, et al. Inherited glaucoma in DBA/2J mice: pertinent disease features for studying the neurodegeneration. *Vis Neurosci*. 2005;22:637–648.
26. Anderson MG, Nair KS, Amonoo LA, et al. GpnmbR 150Xallele must be present in bone marrow derived cells to mediate DBA/2J glaucoma. *BMC Genet*. 2008;9:30.
27. Nair KS, Barbay J, Smith RS, Masli S, John SW. Determining immune components necessary for progression of pigment dispersing disease to glaucoma in DBA/2J mice. *BMC Genet*. 2014;15:42.
28. Turner AJ, Vander Wall R, Gupta V, Klistorner A, Graham SL. DBA/2J mouse model for experimental glaucoma: pitfalls and problems. *Clin Experiment Ophthalmol*. 2017;45:911–922.
29. Sommer A, Tielsch JM, Katz J, et al. Relationship between intraocular pressure and primary open angle glaucoma among white and black Americans. The Baltimore Eye Survey. *Arch Ophthalmol*. 1991;109:1090–1095.
30. Medeiros FA. Biomarkers and surrogate endpoints in glaucoma clinical trials. *Br J Ophthalmol*. 2015;99:599–603.
31. Friedman DS, Wilson MR, Liebmann JM, Fechtner RD, Weinreb RN. An evidence-based assessment of risk factors for the progression of ocular hypertension and glaucoma. *Am J Ophthalmol*. 2004;138:19–31.
32. Nadal-Nicolaś FM, Jimeńez-Lopez M, Sobrado-Calvo P, et al. Brn3a as a marker of retinal ganglion cells: qualitative and quantitative time course studies in naïve and optic nerve–injured retinas. *Invest Ophthalmol Vis Sci*. 2009;50:3860–3868.

33. Jiang S-M, Zeng L-P, Zeng J-H, Tang L, Chen X-M, Wei X. β-III-Tubulin: a reliable marker for retinal ganglion cell labeling in experimental models of glaucoma. *Int J Ophthalmol*. 2015;8:643–652.
34. Zhou Y, Grinchuk O, Tomarev SI. Transgenic mice expressing the Tyr437His mutant of human myocilin protein develop glaucoma. *Invest Ophthalmol Vis Sci*. 2008;49:1932–1939.
35. Sellés-Navarro I, Villegas-Pérez MP, Salvador-Silva M, Ruiz-Gómez JM, Vidal-Sanz M. Retinal ganglion cell death after different transient periods of pressure-induced ischemia and survival intervals. A quantitative in vivo study. *Invest Ophthalmol Vis Sci*. 1996;37:2002–2014.
36. Sung KR, Cho JW, Lee S, et al. Characteristics of visual field progression in medically treated normal-tension glaucoma patients with unstable ocular perfusion pressure. *Invest Ophthalmol Vis Sci*. 2011;52:737–743.
37. Leske MC. Ocular perfusion pressure and glaucoma: clinical trial and epidemiologic findings. *Curr Opin Ophthalmol*. 2009;20:73–78.
38. Gale NW, Thurston G, Hackett SF, et al. Angiopoietin-2 is required for postnatal angiogenesis and lymphatic patterning, and only the latter role is rescued by angiopoietin-1. *Dev Cell*. 2002;3:411–423.
39. Chu M, Li T, Shen B, et al. Angiopoietin receptor Tie2 is required for vein specification and maintenance via regulating COUP-TFII. *Elife*. 2016;5:e21032.
40. Suri C, McClain J, Thurston G, et al. Increased vascularization in mice overexpressing angiopoietin-1. *Science*. 1998;282:468–471.
41. Thurston G, Wang Q, Baffert F, et al. Angiopoietin 1 causes vessel enlargement, without angiogenic sprouting, during a critical developmental period. *Development*. 2005;132:3317.
42. Park DY, Lee J, Kim J, et al. Plastic roles of pericytes in the blood-retinal barrier. *Nat Commun*. 2017;8:15296.
43. Macosko Evan Z, Basu A, Satija R, et al. Highly parallel genome-wide expression profiling of individual cells using nanoliter droplets. *Cell*. 2015;161:1202–1214.
44. Aihara M, Lindsey JD, Weinreb RN. Experimental mouse ocular hypertension: establishment of the model. *Invest Ophthalmol Vis Sci*. 2003;44:4314–4320.
45. Sappington RM, Carlson BJ, Crish SD, Calkins DJ. The microbead occlusion model: a paradigm for induced ocular hypertension in rats and mice. *Invest Ophthalmol Vis Sci*. 2010;51:207–216.